ACS APPLIED MATERIALS & INTERFACES

Research Article

www.acsami.org

Alkyl-Chain-Grafted Hexagonal Boron Nitride Nanoplatelets as Oil-Dispersible Additives for Friction and Wear Reduction

Sangita Kumari,[†] Om P. Sharma,[†] Rashi Gusain,[†] Harshal P. Mungse,[†] Aruna Kukrety,[†] Niranjan Kumar,[‡] Hiroyuki Sugimura,[§] and Om P. Khatri*[,†]

[†]Chemical Science Division, CSIR-Indian Institute of Petroleum (CSIR-IIP), Mohkampur, Dehradun 248005, India

[‡]Materials Science Group, Indira Gandhi Centre for Atomic Research, Kalpakkam 603102, India

[§]Department of Materials Science and Engineering, Kyoto University, Sakyo, Kyoto 606 8501, Japan

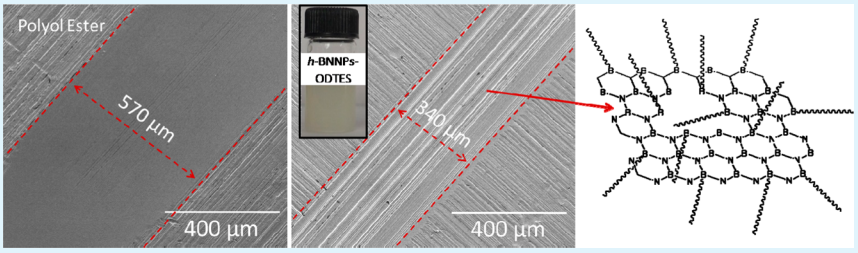

ABSTRACT: Hexagonal boron nitride (*h*-BN), an isoelectric analogous to graphene multilayer, can easily shear at the contact interfaces and exhibits excellent mechanical strength, higher thermal stability, and resistance toward oxidation, which makes it a promising material for potential lubricant applications. However, the poor dispersibility of *h*-BN in lube base oil has been a major obstacle. Herein, *h*-BN powder was exfoliated into *h*-BN nanoplatelets (*h*-BNNPs), and then long alkyl chains were chemically grafted, targeting the basal plane defect and edge sites of *h*-BNNPs. The chemical and structural features of octadecyltriethoxysilane-functionalized *h*-BNNPs (*h*-BNNPs-ODTES) were studied by FTIR, XPS, XRD, HRTEM, and TGA analyses. The *h*-BNNPs-ODTES exhibit long-term dispersion stability in synthetic polyol ester lube base oil because of van der Waals interaction between the octadecyl chains of *h*-BNNPs-ODTES and alkyl functionalities of polyol ester. Micro- and macrotribology results showed that *h*-BNNPs-ODTES, as an additive to synthetic polyol ester, significantly reduced both the friction and wear of steel disks. Elemental mapping of the worn area explicitly demonstrates the transfer of *h*-BNNPs-ODTES on the contact interfaces. Furthermore, insight into the lubrication mechanism for reduction in both friction and wear is deduced based on the experimental results.

KEYWORDS: *boron nitride nanoplatelets, exfoliation, chemical functionalization, dispersion, friction*

INTRODUCTION

Two-dimensional nanomaterials have attracted great attention because of their extraordinary physical and mechanical properties and have shown immense potential for a large range of applications since the invention of graphene.[1] The hexagonal boron nitride (*h*-BN), an isoelectric analogous to graphite, consists of atomically thin sheets of BN. In each sheet of *h*-BN, boron and nitrogen are covalently arranged in a hexagonal structure. Over the past few years, *h*-BN nanosheet, also known as "white graphene", has emerged as a promising nanomaterial for widespread applications owing to unique optical, electrical, mechanical, thermal, and chemical properties. These characteristics are in many cases different from- and superior to the graphene.[2−6] The *h*-BN is an insulator with a wide band gap (~6 eV) and exhibits higher thermal stability and resistance toward oxidation compared to graphene. These intrinsic properties promise the potential of *h*-BN nanosheets for numerous applications including ultraviolet nanoelectronics, piezoelectric, electron field emission, polymeric composites, catalysis supports, self-cleaning coating, etc.[7−13] The weak van der Waals interaction between loosely stacked *h*-BN sheets eases the shearing along the basal plane of its crystalline lamellar structure under the sliding stress and provides excellent lubrication characteristics.[14−16] Therefore, *h*-BN powder (~10^2−10^4 nm size), as an additive to lubricants, improves the antiwear and frictional properties.[16,17] However, most of these studies have certain drawbacks, including the bulkier size of *h*-BN particles and their poor dispersion stability.

Nanoscale friction characteristics of the *h*-BN thin sheets deposited onto a silicon oxide substrate showed that friction monotonically decreased as the number of layers increased and eventually approached that of bulk *h*-BN.[18] Recently, it was further revealed that even a single sheet of *h*-BN can reduce the friction significantly.[19] The mechanical properties of a *h*-BN sheet, particularly Young's modulus and tensile strength, play a significant role, while this material is under contact stress. The two-dimensional bulk modulus of *h*-BN is found to be approximately 80% of the value for the graphene and provides

Received: November 26, 2014
Accepted: January 27, 2015
Published: January 27, 2015

DOI: 10.1021/am5083232
ACS Appl. Mater. Interfaces 2015, 7, 3708−3716

Scheme 1. (a) Digital Image of *h*-BN Powder, (b) Ultrasound-Assisted Exfoliation of *h*-BN Powder into Nanoplatelets,[a] (c) Harsh Oxidation of *h*-BNNPs Using H_2SO_4, $NaNO_3$, and $KMnO_4$ as Oxidizing Reagents, and (d) *h*-BNNPs-ODTES Prepared by Chemical Grafting of ODTES, Targeting the Hydroxyl and Defects Sites of Oxidized *h*-BNNPs

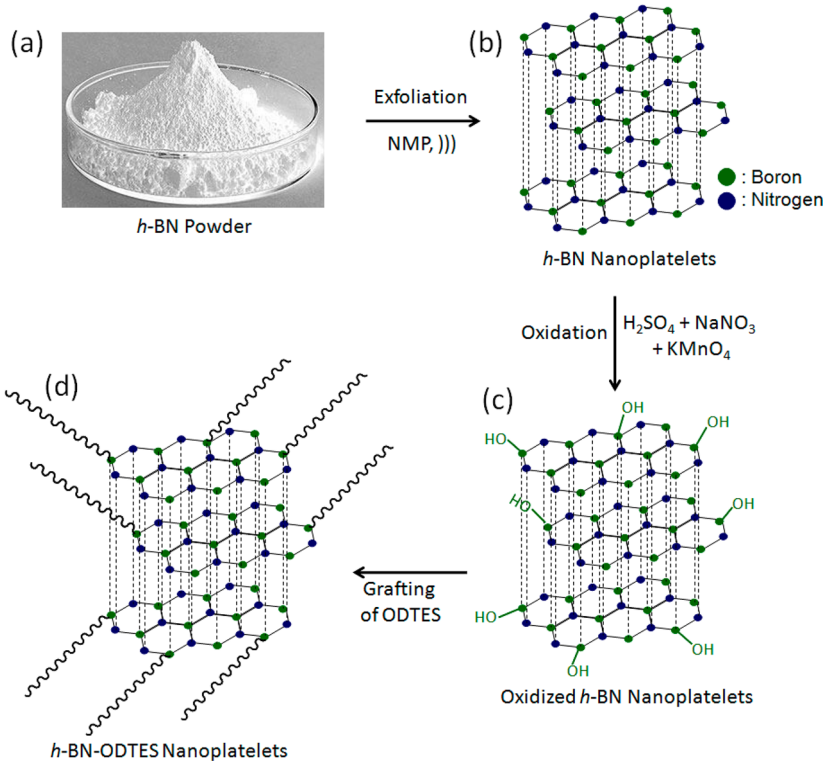

[a]Green and blue spheres represent boron and nitrogen atoms, respectively.

excellent mechanical properties.[6] Over the past few years, chemically functionalized graphene as an additive to lubricating oils has shown excellent tribological characteristics, owing to their layered structure and dispersion stability in the lube media.[20−22] However, *h*-BN tends to agglomerate because of its poor compatibility with lube oils, and that limits the potential of *h*-BN nanosheets for liquid lube applications.

Unlike graphene, the *h*-BN nanosheets possess resistivity toward oxidation and show limited scope for chemical functionalization. Zeng et al. have theoretically investigated that boron nitride nanotubes (BNNTs) can interact with ammonia and amino functional groups carrying compounds.[23] The chemical functionalization of BNNTs with (a) amino-terminated poly(ethylene glycol), (b) ionic liquids through cation−π interaction, and (c) Lewis bases such as trialkylamines and trialkylphosphines were exploited for their dispersion in water and organic solvents.[24−26] Recently, Lin et al. have demonstrated the direct correlation between increasing defect sites of *h*-BN nanosheets and improved reaction efficiency with the alkylamines.[27,28] The chemical interaction between the alkylamine and *h*-BN scaffold is based on the Lewis base−Lewis acid interaction, where the presence of a lone-pair electron in nitrogen of alkylamine functions as Lewis base and vacant p orbitals of boron (Lewis acid) in BNNTs accept the electron pair. Nevertheless, the chemical functionalization of *h*-BN nanosheets with high grafting density is required for their utilization in lubrication applications. The defect and edge sites of *h*-BN nanosheets and nanotubes could be oxidized and generate active hydroxyl functionalities by oxidation with H_2O_2, HNO_3/H_2SO_4, and oleum.[29−31] These functionalities can be further targeted for the task-specific chemical functionalization.

Herein, exfoliation of the *h*-BN powder into *h*-BN nanoplatelets (*h*-BNNPs) was carried out by an ultrasonic probe,[11,32] and then oxygen functionalities were generated by the harsh oxidation of *h*-BNNPs. The developed oxidized material was chemically functionalized with long alkyl chain molecules and dispersed in synthetic lube base oil. The tribological properties of long-alkyl-chain-grafted *h*-BNNPs were investigated by measuring the friction coefficient and wear. Further, the lubrication mechanism is proposed on the basis of the thorough characterization of worn surfaces.

EXPERIMENTAL SECTION

Preparation of Oxidized *h*-BNNPs. The *h*-BN powder with an average particle size of 70 nm was procured from MK Impex Canada. A total of 1.0 g of *h*-BN powder was sonicated (Scheme 1a,b) in 500 mL of *N*-methylpyrrolidone (NMP) using an ultrasonication probe (Sonics Vibra-cell, VCX 500, 40% intensity, tip diameter 13 mm, temperature cutoff 70 °C) for 2 h in the pulse mode. After sonication, the suspension of *h*-BN in NMP was kept overnight to allow the nonexfoliated content of the *h*-BN powder to settle. The supernatant having stable dispersion of *h*-BNNPs in NMP was decanted and centrifuged at 5000 rpm for 15 min. The deposited material in the centrifuge tubes comprised *h*-BNNPs, which was then washed with ethanol and dried in an air oven (60 °C). In the next step, *h*-BNNPs were oxidized under strong oxidizing conditions to generate the oxygen functionalities on the defect and edge sites of the material (Scheme 1c). In a typical set of experiment, 0.5 g of *h*-BNNPs was added to a round-bottomed flask containing 24 mL of H_2SO_4 and 0.5 g of sodium nitrate under a controlled temperature of 4 °C. This was followed by the gradual addition of 3 g of $KMnO_4$ in the reaction mixture, and the temperature of the reaction vessel was maintained below 4 °C. Thereafter, the reaction mixture was allowed to set for oxidation of *h*-BNNPs under uninterrupted stirring for 24 h at room

DOI: 10.1021/am5083232
ACS Appl. Mater. Interfaces 2015, 7, 3708−3716

temperature. Subsequently, 24 mL of distilled water was gradually added to the reaction mixture, and the temperature of the reaction vessel was raised to 98 °C using an oil bath. After 48 h, the reaction mixture was rinsed with H_2O_2 (30%) and then with HCl (3.5%). This was followed by several washings of the reaction product using distilled water, until neutral pH was attained. In the final step, the oxidized product was separated out by membrane filtration under a vacuum line and dried in an air oven (100 °C).

Chemical Functionalization of *h*-BNNPs. A total of 0.5 g of oxidized *h*-BNNPs was dispersed in 62.5 mL of toluene using an ultrasonic bath. Prior to chemical functionalization, oxidized *h*-BNNPs dispersion was purged with nitrogen gas. This was followed by the addition of 1.75 mL of octadecyltriethoxysilane (ODTES). The reaction mixture was refluxed for 24 h under a nitrogen atmosphere. The developed material (*h*-BNNPs-ODTES) was then thoroughly washed with toluene (three times) and then with ethanol (two times) to remove all of the nonreacted content of ODTES. *h*-BNNPs-ODTES was dried in an air oven, prior to their chemical and structural characterization.

Chemical and Structural Characterization. Fourier transform infrared (FTIR) transmittance spectra of all samples (KBr pellets) were recorded using a Thermo Scientific Nicolet 8700 research spectrometer with a resolution of 4 cm^{-1}. X-ray photoelectron spectroscopy (XPS; JPS-9010TRX, JEOL Ltd.) measurements were carried out using thin films of each sample, and the chemical changes were probed. All XPS measurements were recorded using a Mg Kα line as the X-ray source. The peak fitting of the B 1s and C 1s spectra was carried out by using a Gaussian−Lorentzian function after performing a Shirley background correction. Powder X-ray diffraction (XRD) analyses of all samples were carried out using a Bruker D8 Advanced diffractometer at 40 kV and 40 mA using Cu Kα radiation (λ = 0.15418 nm). Diffraction data were recorded for a 2θ angle between 2° and 80° (step size 0.020°; step time 1 s). Thermogravimetric analysis (TGA) of the samples was carried out using a thermal analyzer (Diamond, PerkinElmer). Samples were analyzed in the temperature range of 30−800 °C at a thermal rate of 10 °C/min under a steady flow of nitrogen. High-resolution transmission electron microscopy (HRTEM) analysis of all samples was carried out on a JEOL 3010 electron microscope at 300 kV by drop casting of their ethanolic dispersion on the TEM grid.

Friction and Wear Test Procedures. The tribological properties in terms of the friction coefficient and wear were measured using a ball-on-disk NTR2 microtribometer and standard tribometer (CSM Instruments, Peseux, Switzerland) operating in uni- and bidirectional modes, respectively. In NTR2 microtribometer and standard tribometer experiments, 100Cr6 steel balls (ϕ = 2 and 6 mm, respectively) were used as sliding materials against the lubricated steel (100Cr6 and 316LN, respectively) disks. One drop of lubricant was applied between the contact interfaces, ensuring that lubricant is always present between the sliding interfaces. Pentaerythritol tetraoleate ester (polyol ester) was used as the reference lube oil throughout this study. In a NTR2 microtribometer, all experiments were carried out at a normal applied load of 250 mN and a linear speed of 1 cm/s for the 500 laps. The NTR2 microtribometer is equipped with two independent high-resolution capacitive sensors for normal and friction forces. In standard tribometer experiments, a sliding ball is mounted in a holder, which is connected through a stiff lever coupled with a friction force transducer. The sliding speed and load were kept constant at 3 cm/s and 2 N, respectively. Two-dimensional wear profiles of worn areas were measured by a Dektak 6M stylus profiler with fixed 5 mg contact load and 10 μm/s scanning speed. In this method, the tip of the diamond stylus was scanned across the wear track, generating a two-dimensional wear profile. The stylus was mechanically coupled to the core of an LVDT sensor. The morphological and elemental features on the worn areas were examined by using field-emission scanning electron microscopy (FESEM; FEI Quanta 200 F) coupled with energy-dispersive X-ray spectroscopy (EDX).

RESULTS AND DISCUSSION

The *h*-BN powder was exfoliated into *h*-BNNPs by using an ultrasonic probe and then rigorously oxidized to generate active

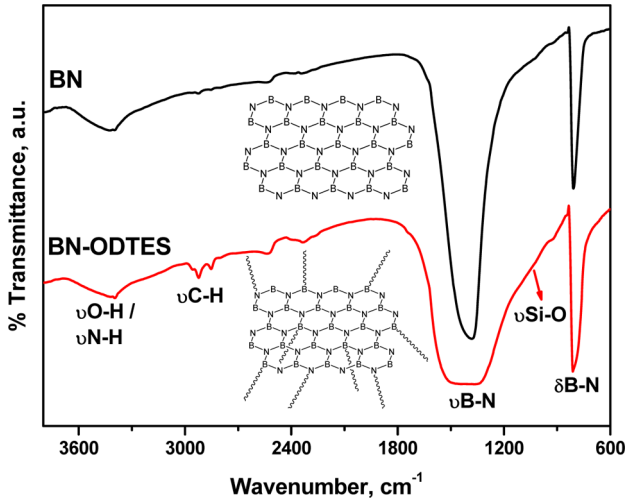

Figure 1. FTIR spectra of the *h*-BN powder and *h*-BNNPs-ODTES along with their vibrational assignments.

sites for their chemical functionalization. The surface-active ODTES was then grafted on *h*-BNNPs by targeting their oxygen functionalities and defect sites. The chemical and structural changes that occurred during the exfoliation, oxidation, and then chemical interaction of ODTES molecules with *h*-BNNPs were thoroughly monitored by FTIR, XPS, TGA, XRD, and HRTEM analyses. Figure 1 shows vibrational spectra of the *h*-BN powder and *h*-BNNPs-ODTES along with their characteristic vibrational assignments. The *h*-BN powder exhibits (a) a strong and sharp absorption peak at 808 cm^{-1}, attributed to the out-of-plane B−N−B bending mode, and (b) a very broad and strong vibration peak centered at 1382 cm^{-1}, ascribed to the in-plane B−N stretching mode.[13,33] A broad peak appearing at ∼3400 cm^{-1} in the *h*-BN powder is assigned to the surface moisture along with traces of hydroxyl and amino groups at the edges of *h*-BN. Besides characteristic vibrational signatures of the *h*-BN scaffold, *h*-BNNPs-ODTES showed strong vibrational modes in the range of 3000−2800 cm^{-1}, attributed to the C−H stretches of methylene and methyl groups, suggesting the grafting of alkyl chains on *h*-BNNPs.

XPS is a very powerful analysis tool for the detection of the chemical state of elements and their stoichiometry in the material. Figure 2 shows the high-resolution B 1s, N 1s, C 1s, and Si 2p XPS spectra of *h*-BNNPs-ODTES. The B 1s and N 1s peaks are located at 190.6 and 398.2 eV, respectively. The observed values are in good agreement with the literature values.[29,34] The B 1s spectrum of *h*-BNNPs-ODTES could be deconvoluted into two chemically shifted components at 190.6 and 192.1 eV (Figure 2a). These peaks are attributed to the B−N linkage of the *h*-BN scaffold with very strong intensity and the B−O linkage with very low peak intensity, respectively. XPS calculation showed the ratio of B−O/B−N = 0.03, demonstrating that ∼3% of the boron atoms, which are located on the edge and defect sites in the surface layer of *h*-BNNPs, are oxidized into B−OH groups. Furthermore, the atomic percentages of boron and nitrogen in pristine *h*-BN powder and *h*-BNNPs-ODTES were calculated based on XPS study to determine the elemental stoichiometry. The ratio of B/N =

DOI: 10.1021/am5083232
ACS Appl. Mater. Interfaces 2015, 7, 3708−3716

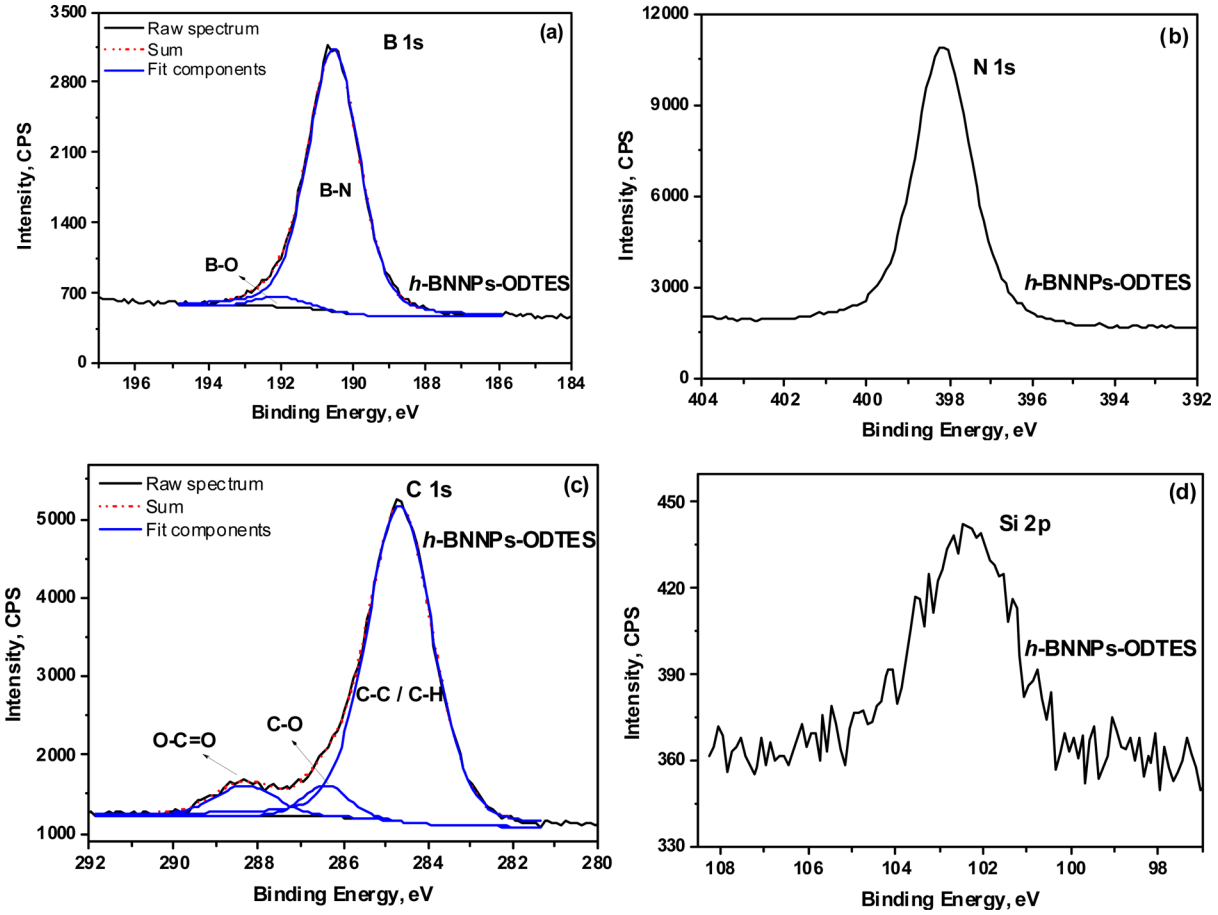

Figure 2. High-resolution XPS spectra of the (a) B 1s, (b) N 1s, (c) C 1s, and (d) Si 2p regions for *h*-BNNPs-ODTES. The deconvoluted components in B 1s and C 1s spectra illustrate chemical linkage with various types of functionalities in *h*-BNNPs-ODTES.

1.059 in pristine *h*-BN powder was increased to 1.077 in *h*-BNNPs-ODTES, revealing the loss of nitrogen during harsh oxidation. The loading of ODTES on *h*-BNNPs was further confirmed by the appearance of C 1s and Si 2p peaks (Figure 2c,d). The high-resolution C 1s spectrum of *h*-BNNPs-ODTES showed an asymmetric peak structure with a small tail at higher binding energy, attributed to different types of carbon structure. The peak fitting of the C 1s spectrum of *h*-BNNPs-ODTES could be deconvoluted into three chemically shifted components (Figure 2c). The C 1s peak centered at 284.6 eV as a major component is attributed to C−C/C−H carbons and represents the octadecyl group of ODTES grafted on *h*-BNNPs. Two additional overlapped components at 286.4 and 288.5 eV are assigned to the C−O and COO functional groups, respectively. The presence of an ethoxyl functional group in ODTES and environmental contamination during XPS analysis contribute for these two peak components.

Figure 3 depicts the XRD pattern of the *h*-BN powder and *h*-BNNPs-ODTES. The diffraction peaks corresponding to the (002), (100), (101), (102), (004), and (110) planes are characteristic of the *h*-BN powder. The increased full width at half-maximum of the (002) diffraction peak of *h*-BNNPs-ODTES (Figure 3b) confirms the decreased number of layers (thickness reduction), owing to exfoliation of the *h*-BN powder. The three-dimensional order of the *h*-BN powder and *h*-BNNPs-ODTES was measured by calculating the graphitizing index (GI) using the (100), (101), and (102) XRD peak parameters.[35] Increased intensity of the (102) peak revealed the improved three-dimensional order. In general, the *h*-BN powder with a GI value of 1.6 is considered to have perfect three-dimensional order and represents the highly ordered stacking of *h*-BN layers along the *c* axis. The improper stacking and rotation of layers along the *c* axis lead to increased GI and, consequently, a decrease of the three-dimensional order. Herein, a higher value of GI (2.78) for the *h*-BN powder compared to *h*-BNNPs-ODTES (GI = 1.90) suggests that, during the ultrasound-facilitated exfoliation, the *h*-BN powder exfoliates at the point of their disordered stacking and leads to *h*-BNNPs with relatively ordered structure. Figure 4 shows HRTEM images of pristine *h*-BN powder and *h*-BNNPs-ODTES. The lateral thickness of pristine *h*-BN powder is in the range of 20−60 nm (Figure 4a_i−a_{iii}). The microscopic observations suggested that *h*-BNNPs-ODTES, prepared by exfoliation of the *h*-BN nanopowder and then grafting of ODTES, exhibited a relatively low number of layers. The thickness of these nanoplatelets is noted to be in the range of 5−20 nm (Figure 4b_{iii}). Under high resolution, parallel-line features of *h*-BNNPs-ODTES are observed with an interlayer distance of ∼0.35 nm, consistent with the XRD results. TGA was carried out to probe the thermal decomposition property of grafted ODTES molecules. Pristine BN powder showed 2.5 wt % loss up to 330 °C, attributed to the absorbed contamination (Figure 5), while *h*-BNNPs-ODTES exhibited 4 wt % loss up to 550 °C and was attributed to the degradation of ODTES.

The *h*-BN powder is nondispersible in various lubes and tends to agglomerate and settle down owing to their bulkier

DOI: 10.1021/am5083232
ACS Appl. Mater. Interfaces 2015, 7, 3708−3716

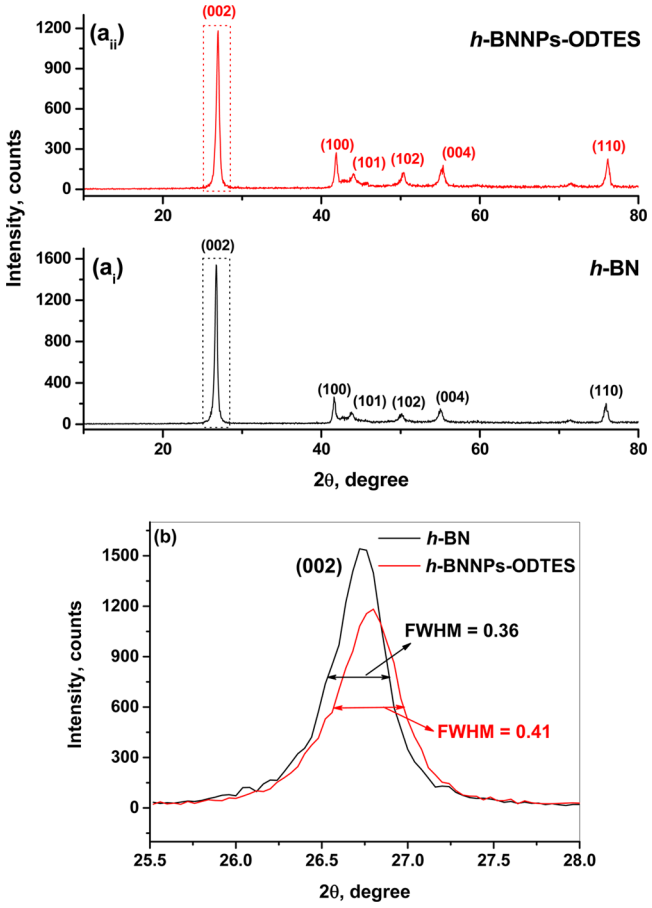

Figure 3. XRD patterns of (a_i) the *h*-BN powder and (a_{ii}) *h*-BNNPs-ODTES. (b) Expanded region of the superimposed (002) diffraction peak of the *h*-BN powder and *h*-BNNPs-ODTES, illustrating the broadening effect attributed to the thinning of *h*-BN nanoparticles.

particle size and the difference in cohesive energies between the material and lubes. However, for efficient tribological performance, *h*-BNNPs must be thoroughly dispersed in applicable

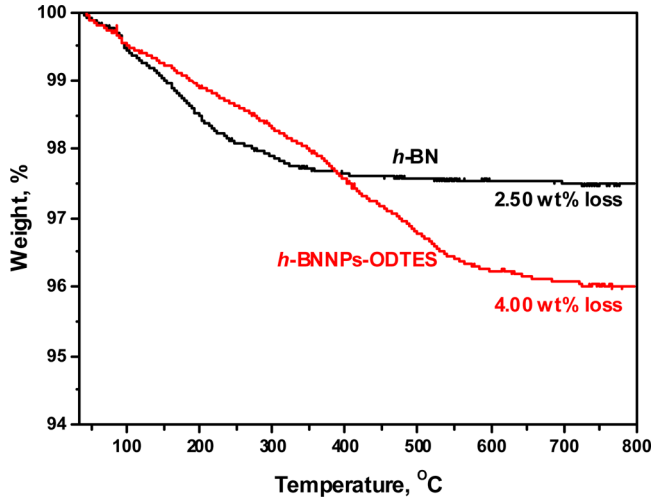

Figure 5. TGA patterns of the *h*-BN powder and *h*-BNNPs-ODTES over the temperature range of 35−800 °C under a nitrogen flow.

lubes. Figure 6 shows digital images of the dispersion of *h*-BNNPs-ODTES in polyol ester lube base oil as a function of time. Dispersion of *h*-BNNPs-ODTES is found to be stable. Its long-term dispersion stability was attributed to (a) van der Waals interaction between the long alkyl chains grafted on *h*-BNNPs and the alkyl chains of polyol ester (pentaerythritol tetraoleate) and (b) the high specific surface area of *h*-BNNPs-ODTES.

The tribological properties of *h*-BNNPs-ODTES were evaluated using polyol ester as a lube base oil for the steel−steel sliding contacts. Figure 7 shows (a) changes of the friction coefficient with the number of laps and (b) the average friction coefficient for different concentrations of *h*-BNNPs-ODTES blended in polyol ester under the Hertzian contact pressure of 864 MPa. Polyol ester, which is considered to be a highly stable and biodegradable synthetic lube base oil, exhibited ∼0.125 friction coefficient. Figure 7b shows that the average friction coefficient decreases with increasing concentration of *h*-

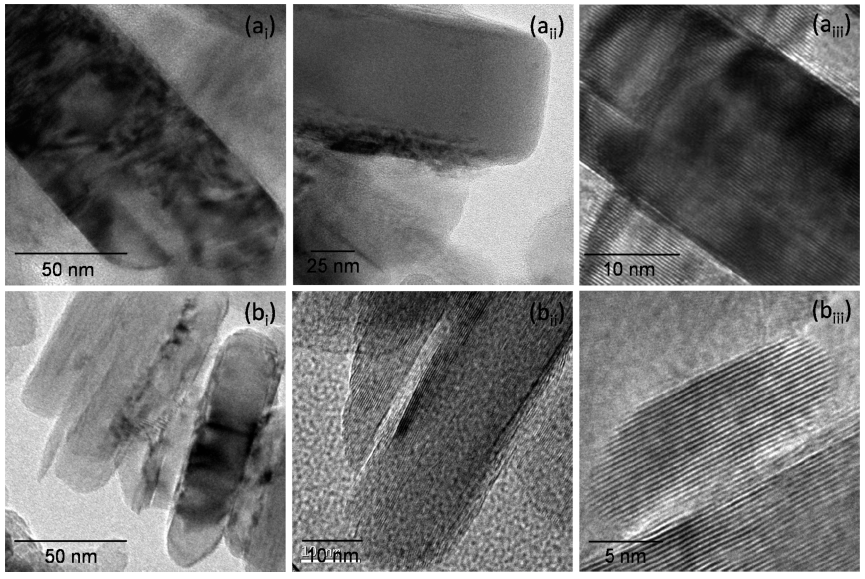

Figure 4. HRTEM images of (a_i−a_{iii}) the *h*-BN powder and (b_i−b_{iii}) *h*-BNNPs-ODTES. The thinning of *h*-BN with a countable number of layers can be explicitly seen in the HRTEM images of *h*-BNNPs-ODTES (b_i−b_{iii}).

DOI: 10.1021/am5083232
ACS Appl. Mater. Interfaces 2015, 7, 3708−3716

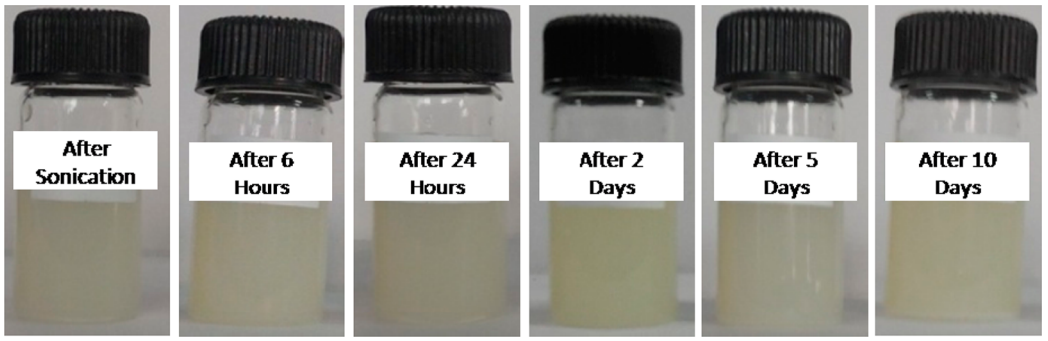

Figure 6. Digital images of dispersion of *h*-BNNPs-ODTES in polyol ester lubricant. The time for each picture is noted on the respective sample bottle. Concentration of *h*-BNNPs-ODTES: 0.25 mg/mL.

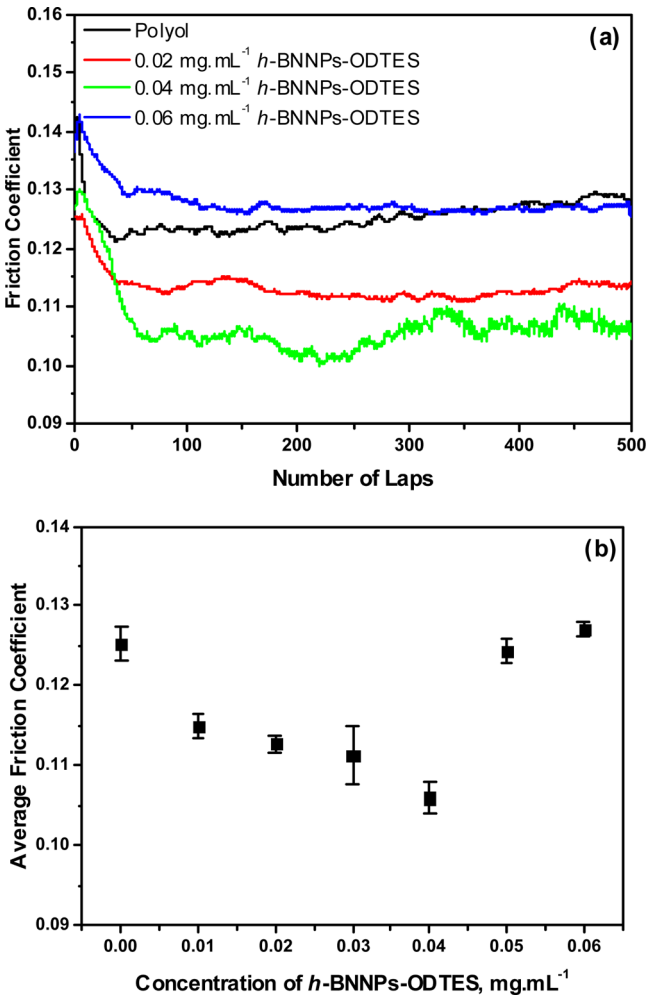

Figure 7. (a) Evolution of the friction coefficient with the number of laps. (b) Changes in the average friction coefficient for polyol ester as a function of increasing doses of *h*-BNNPs-ODTES under unidirectional sliding contact. Conditions: load 250 mN; speed 1 cm/s; Hertzian contact pressure 864 MPa.

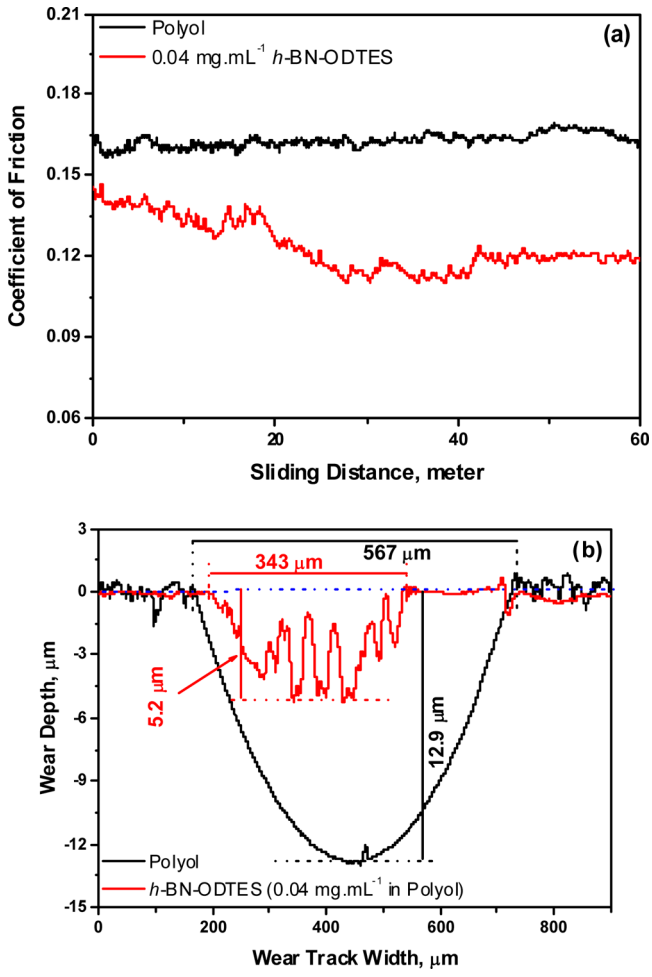

Figure 8. Lubrication characteristics: (a) changes in the friction coefficient and (b) wear parameters of the polyol ester lube oil with and without *h*-BNNPs-ODTES (concentration 0.04 mg/mL) under bidirectional sliding contact. Conditions: load 2 N; speed 3 cm/s; sliding distance 100 m.

BNNPs-ODTES in polyol ester. The lowest friction coefficient was found at a concentration of 0.04 mg/mL. This revealed that *h*-BNNPs-ODTES, used as an additive to polyol ester, remarkably reduces the friction coefficient. Furthermore, higher friction was observed with increasing concentration of *h*-BNNPs-ODTES. Plausibly, the higher concentration of *h*-BNNPs-ODTES between the contact interfaces leads to an abrasive effect. Consequently, there is a high resistance to shear, and that increases the friction.[36] The XRD and HRTEM results (Figures 3 and 4b) revealed that hexagonal lamella of *h*-BNNPs-ODTES are stacked by weak van der Waals interaction with an interlayer spacing of ~3.35 Å. Low resistance to shear between the weakly interacted lamella in *h*-BNNPs-ODTES under the sliding contact stress reduced the friction coefficient. Besides that, stable dispersion of these nanoplatelets in polyol ester ensured their uninterrupted supply on the tribological

DOI: 10.1021/am5083232
ACS Appl. Mater. Interfaces 2015, 7, 3708−3716

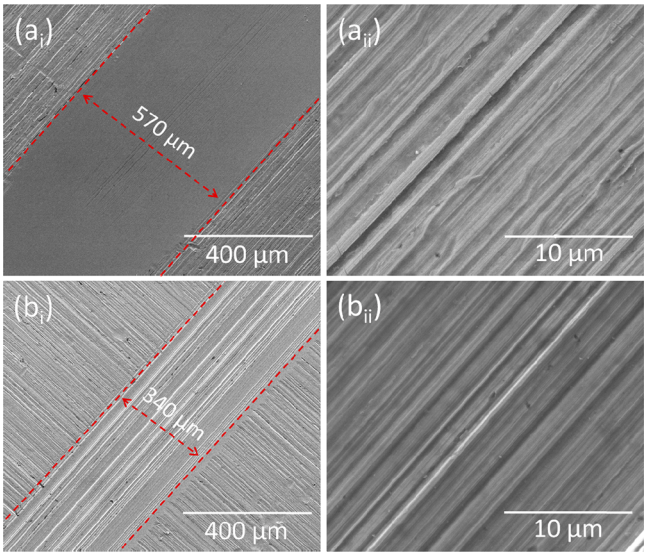

Figure 9. Microscopic images of the worn track on a steel disk after lubrication tests under a 2 N load. Prior to microscopic analysis, the steel disks were thoroughly washed to remove the physisorbed content on the materials. (a_i and a_{ii}) Lubricated with polyol ester and (b_i and b_{ii}) lubricated with *h*-BNNPs-ODTES blended polyol ester (dose 0.04 mg/mL).

interfaces. As a result, *h*-BNNPs-ODTES significantly reduced the friction compared to that of polyol ester.

Furthermore, macrotribological tests were conducted to understand the lubrication mechanism. Figure 8a depicts changes in the friction coefficient for steel−steel contact using polyol ester and a *h*-BNNPs-ODTES (0.04 mg/mL) blended polyol sample under a load of 2 N. The results suggest that *h*-BNNPs-ODTES can effectively reduce the friction coefficient. Another important feature studied is the influence of *h*-BNNPs-ODTES on the wear behavior of the contact bodies. Figure 8b shows a representative wear track profile of a steel disk lubricated with polyol ester and a *h*-BNNPs-ODTES sample. The wear track lubricated with polyol ester exhibited ∼570 and 12.9 μm track width and depth, respectively. In the presence *h*-BNNPs-ODTES (0.04 mg/mL), both the wear track width and depth decreased significantly to ∼345 and 5.2 μm, respectively. The microscopic images of wear tracks formed on the steel disk are shown in Figure 9. The FESEM images of a steel disk lubricated with polyol ester exhibited deep scratches and grooves, indicating severe plastic deformation. In the presence of *h*-BNNPs-ODTES, the wear track width decreases by ∼40% and exhibits comparatively smoother features, revealing the wear-resistive property of *h*-BNNPs-ODTES against the material damages. EDX analysis on the worn surfaces of a steel disk was further carried out for probing the qualitative elemental estimation on the tribological interfaces. The FESEM micrograph and corresponding abundance of boron and nitrogen on the worn area of a steel disk lubricated with *h*-BNNPs-ODTES (Figure 10) illustrate their uniform distribution. The thorough distribution of boron and nitrogen on the worn areas of a steel disk suggested the deposition of *h*-BNNPs on the contact interface. Although the collected elemental mapping is a qualitative idea, it strongly suggests the role of *h*-BNNPs for improved tribological properties. Drummond et al. demonstrated that layered WS_2 particles as additives to tetradecane sheared between the contact bodies, reducing the friction force and improving the resistance of the surfaces to wear.[37] The shear-induced delamination of WS_2 and subsequent formation of a transfer film of WS_2 on the contact surfaces were found to be responsible for the reduction in friction. Recently, Biswas et al. suggested the friction-induced transfer of MoS_2 layers on the contact interfaces, revealed by in situ total internal reflection Raman tribometer analyses.[38] Herein, the elemental mapping of worn areas strongly suggests the deposition of *h*-BN on the contact interfaces. The gradual reduction of friction during the initial sliding contact (Figure 8a) further suggests the transfer of *h*-BNNPs on the contact interfaces and eventually leads to the regular deposition of a thin film of *h*-BNNPs. This is supported by the low value of friction and its stabilization after sliding of ∼25 m distance (Figure 8a). The internal shear in the deposited thin films of *h*-BN and slide over the dispersed *h*-BNNPs-ODTES under the contact stress reduces the friction and protects the contact interfaces from damage. This study demonstrates that a very low dose (40 ppm) of nicely dispersed *h*-BNNPs-ODTES can generate the *h*-BN tribological thin film, which could efficiently reduce the friction and protect the sliding interfaces. This promises the potential of *h*-BNNP-based lubricants for conserving energy by lowering the friction and reduction of material losses (wear-preventive property) for tribological applications.

CONCLUSIONS

Chemical grafting and the dimension/size of nanomaterials are important parameters to control nanomaterial dispersion in the liquid lubricants. Herein, the *h*-BN powder was exfoliated into the *h*-BNNPs, as revealed by HRTEM and XRD. The exfoliated *h*-BNNPs were then rigorously oxidized to generate the hydroxyl groups on the basal plane defect and edge sites. These hydroxyl functionalities are prone to interact with long alkyl chains carrying ODTES through covalent linkage. The exfoliation, oxidation, and then chemical grafting of ODTES on the *h*-BNNPs were monitored by FTIR, XPS, XRD, HRTEM, and TGA. The presence of octadecyl chains in *h*-BNNPs-

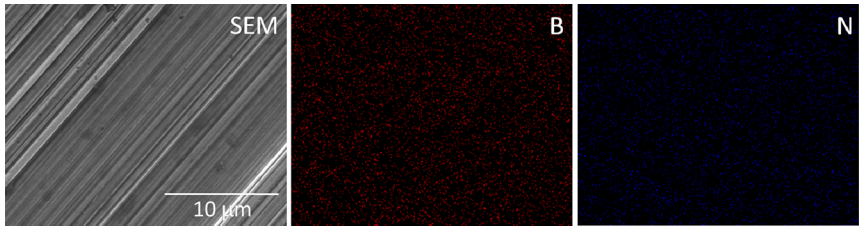

Figure 10. FESEM micrograph and corresponding elemental mapping on the worn track of a steel disk lubricated with *h*-BNNPs-ODTES blended with polyol ester (dose 0.04 mg/mL). The uniform distribution of boron and nitrogen on the worn track of a steel disk revealed the deposition of *h*-BNNPs on the tribological interfaces.

DOI: 10.1021/am5083232
ACS Appl. Mater. Interfaces 2015, 7, 3708−3716

ODTES facilitated their dispersion in polyol ester lube base oil. The van der Waals interaction between the alkyl chains grafted on *h*-BNNPs-ODTES and the hydrocarbon groups of polyol ester plays a crucial role and provides long-term dispersion stability. The tribological results showed that *h*-BNNPs-ODTES in polyol ester significantly improves the lubricity by reducing the friction and wear parameters. The lubricity enhancement was attributed to low resistance to shear provided by the weakly stacked lamellar structure of *h*-BNNPs-ODTES. Elemental mapping on the wear track of a steel disk suggested the development of a *h*-BN thin film on the contact interfaces. The internal shear in the deposited thin films of *h*-BN and slide over the dispersed *h*-BNNPs-ODTES under the contact stress reduces the friction and protects the contact interfaces from damage. This study demonstrates that thoroughly dispersed *h*-BNNPs-ODTES can significantly improve the tribological properties of the lubricant by reducing the friction and wear.

AUTHOR INFORMATION

Corresponding Author

*E-mail: opkhatri@iip.res.in. Fax: +91 135 2660200.

Funding

Council of Scientific and Industrial Research, Government of India.

Notes

The authors declare no competing financial interest.

ACKNOWLEDGMENTS

We kindly acknowledge the Director of CSIR-IIP for his kind permission to publish these results. The authors are thankful to CSIR, India, for financial support through the 12th FYP project (CSC-118/04). The authors are also grateful to Analytical Science Division of CSIR-IIP, Dehradun; DST unit of Nanoscience, IIT Madras, Chennai; Ashok Bahuguna of IGCAR, Kalpakkam, for providing their help in various measurements. R.G. and H.P.M. thank the CSIR and UGC, India, respectively, for fellowship support.

REFERENCES

(1) Novoselov, K. S.; Geim, A. K.; Morozov, S. V.; Jiang, D.; Dubonos, S. V.; Grigorieva, L. V.; Firsov, A. A. Electric Field Effect in Atomically Thin Carbon Films. *Science* **2004**, *306*, 666−669.

(2) Zeng, H.; Zhi, C.; Zhang, Z.; Wei, X.; Wang, X.; Guo, W.; Bando, Y.; Golberg, D. "White Graphenes": Boron Nitride Nanoribbons via Boron Nitride Nanotube Unwrapping. *Nano Lett.* **2010**, *10*, 5049−5055.

(3) Pakdel, A.; Bando, Y.; Golberg, D. Nano Boron Nitride Flatland. *Chem. Soc. Rev.* **2014**, *43*, 934−959.

(4) Meng, W.; Huang, Y.; Fu, Y.; Wang, Z.; Zhi, C. Polymer Composites of Boron Nitride Nanotubes and Nanosheets. *J. Mater. Chem. C* **2014**, *2*, 10049−10061.

(5) Nag, A.; Raidongia, K.; Hembram, K. P. S. S.; Datta, R.; Waghmare, U. V.; Rao, C. N. R. Graphene Analogues of BN: Novel Synthesis and Properties. *ACS Nano* **2010**, *4*, 1539−1544.

(6) Andrew, R. C.; Mapasha, R. E.; Ukpong, A. M.; Chetty, N. Mechanical Properties of Graphene and Boronitrene. *Phys. Rev. B* **2012**, *85*, 125428.

(7) Watanabe, K.; Taniguchi, T.; Kanda, H. Direct-bandgap Properties and Evidence for Ultraviolet Lasing of Hexagonal Boron Nitride Single Crystal. *Nat. Mater.* **2004**, *3*, 404−409.

(8) Duerloo, K. A. N.; Reed, E. J. Flexural Electromechanical Coupling: A Nanoscale Emergent property of Boron Nitride Bilayers. *Nano Lett.* **2013**, *13*, 1681−1686.

(9) Chen, Z. G.; Zou, J. Field Emitters: Ultrathin BN Nanosheets Protruded From BN Fibers. *J. Mater. Chem.* **2011**, *21*, 1191−1195.

(10) Dean, C. R.; Young, A. F.; Meric, I.; Lee, C.; Wang, L.; Sorgenfrei, S.; Watanabe, K.; Taniguchi, T.; Kim, P.; Shepard, K. L.; Hone, J. Boron Nitride Substrates for High-quality Graphene Electronics. *Nat. Nanotechnol.* **2010**, *5*, 722−726.

(11) Zhi, C.; Bando, Y.; Tang, C.; Kuwahara, H.; Golberg, D. Large-Scale Fabrication of Boron Nitride Nanosheets and Their Utilization in Polymeric Composites with Improved Thermal and Mechanical Properties. *Adv. Mater.* **2009**, *21*, 2889−2893.

(12) Gao, M.; Lyalin, A.; Taketsugu, T. Catalytic Activity of Au and Au_2 on the h-BN Surface: Adsorption and Activation of O_2. *J. Phys. Chem. C* **2012**, *116*, 9054−9062.

(13) Yu, J.; Qin, L.; Hao, Y.; Kuang, S.; Bai, X.; Chong, Y.-M.; Zhang, W.; Wang, E. Vertically Aligned Boron Nitride Nanosheets: Chemical Vapor Synthesis, Ultraviolet Light Emission, and Superhydrophobicity. *ACS Nano* **2010**, *4*, 414−422.

(14) Deacon, R. F.; Goodman, J. F. Lubrication by Lamellar Solids. *Proc. R. Soc. London* **1958**, *243*, 464−482.

(15) Rowe, G. W. Some Observations on the Frictional Behaviour of Boron Nitride and of Graphite. *Wear* **1960**, *3*, 274−285.

(16) Kimura, Y.; Wakabayashi, T.; Okada, K.; Wada, T.; Nishikawa, H. Boron Nitride as a Lubricant Additive. *Wear* **1999**, *232*, 199−206.

(17) Celik, O. N.; Ay, N.; Goncu, Y. Effect of Nano Hexagonal Boron Nitride Lubricant Additives on the Friction and Wear Properties of AISI 4140 Steel. *Part. Sci. Technol.* **2013**, *31*, 501−506.

(18) Lee, C.; Li, Q.; Kalb, W.; Liu, X. Z.; Berger, H.; Carpick, R. W.; Hone, J. Frictional Characteristics of Atomically Thin Sheets. *Science* **2010**, *328*, 76−80.

(19) Li, X.; Yin, J.; Zhou, J.; Guo, W. Large Area Hexagonal Boron Nitride Monolayer as Efficient Atomically Thick Insulating Coating Against Friction and Oxidation. *Nanotechnology* **2014**, *25*, 105701.

(20) Choudhary, S.; Mungse, H. P.; Khatri, O. P. Dispersion of Alkylated Graphene in Organic Solvents and Its Potential for Lubrication Applications. *J. Mater. Chem.* **2012**, *22*, 21032−21039.

(21) Berman, D.; Erdemir, A.; Sumant, A. V. Graphene: A New Emerging Lubricant. *Mater. Today* **2014**, *17*, 31−42.

(22) Mungse, H. P.; Khatri, O. P. Chemically Functionalized Reduced Graphene Oxide as a Novel Material for Reduction of Friction and Wear. *J. Phys. Chem. C* **2014**, *118*, 14394−14402.

(23) Wu, X.; An, W.; Zeng, X. C. Chemical Functionalization of Boron-Nitride Nanotubes with NH_3 and Amino Functional Groups. *J. Am. Chem. Soc.* **2006**, *128*, 12001−12006.

(24) Xie, S. Y.; Wang, W.; Fernando, K. A. S.; Wang, X.; Lin, Y.; Sun, Y. P. Solubilization of Boron Nitride Nanotubes. *Chem. Commun.* **2005**, 3670−3672.

(25) Zhi, C.; Bando, Y.; Wang, W.; Tang, C.; Kuwahara, H.; Golberg, D. Molecule Ordering Triggered by Boron Nitride Nanotubes and "Green" chemical Functionalization of Boron Nitride Nanotubes. *J. Phys. Chem. C* **2007**, *111*, 18545−18549.

(26) Shrinwantu, P.; Vivekchand, S. R. C.; Govindaraj, A.; Rao, C. N. R. Functionalization and Solubilization of BN Nanotubes by Interaction with Lewis Bases. *J. Mater. Chem.* **2007**, *17*, 450−452.

(27) Lin, Y.; Williams, T. V.; Connell, J. W. Soluble, Exfoliated Hexagonal Boron Nitride Nanosheets. *J. Phys. Chem. Lett.* **2010**, *1*, 277−283.

(28) Lin, Y.; Williams, T. V.; Cao, W.; Elsayed-Ali, H. E.; Connell, J. W. Defect Functionalization of Hexagonal Boron Nitride Nanosheets. *J. Phys. Chem. C* **2010**, *114*, 17434−17439.

(29) Nazarov, A. S.; Demin, V. N.; Grayfer, E. D.; Bulavchenko, A. I.; Arymbaeva, A. T.; Shin, H.-J.; Choi, J.-Y.; Fedorov, V. E. Functionalization and Dispersion of Hexagonal Boron Nitride (h-BN) Nanosheets Treated with Inorganic Reagents. *Chem.—Asian J.* **2012**, *7*, 554−560.

(30) Zhi, C. Y.; Bando, Y.; Terao, T.; Tang, C. C.; Kuwahara, H.; Golberg, D. Chemically Activated Boron Nitride Nanotubes. *Chem.—Asian J.* **2009**, *4*, 1536−1540.

DOI: 10.1021/am5083232
ACS Appl. Mater. Interfaces 2015, 7, 3708−3716

(31) Zhi, Y.; Hanagata, N.; Bando, Y.; Golberg, D. Dispersible Shortened Boron Nitride Nanotubes with Improved Molecule-Loading Capacity. *Chem.—Asian J.* **2011**, *6*, 2530−2535.
(32) Nicolosi, V.; Chhowalla, M.; Kanatzidis, M. G.; Strano, M. S.; Coleman, J. N. Liquid Exfoliation of Layered Materials. *Science* **2013**, *340*, 1420.
(33) Hou, J.; Li, G.; Yang, N.; Qin, L.; Grami, M. E.; Zhang, Q.; Wang, N.; Qu, X. Preparation and Characterization of Surface Modified Boron Nitride Epoxy Composites with Enhanced Thermal Conductivity. *RSC Adv.* **2014**, *4*, 44282−44290.
(34) Shi, Y.; Hamsen, C.; Jia, X.; Kim, K. K.; Reina, A.; Hofmann, M.; Hsu, A. L.; Zhang, K.; Li, H.; Juang, Z. Y.; Dresselhaus, M. S.; Li, L. J.; Kong, J. Synthesis of Few-Layer Hexagonal Boron Nitride Thin Film by Chemical Vapor Deposition. *Nano Lett.* **2010**, *10*, 4234−4139.
(35) Balint, M. G.; Petrescu, M. I. An Attempt to Identify the Presence of Polytype Stacking Faults in hBN Powders by Means of X-ray Diffraction. *Diamond Relat. Mater.* **2009**, *18*, 1157−1162.
(36) Elomaa, O.; Singh, V. K.; iYER, a.; Hakala, T. J.; Koskinen, J. Graphene-oxide in Water Lubrication on Diamond-Like Carbon vs. Stainless Steel High-Load Contacts. *Diamond Relat. Mater.* **2015**, *52*, 43−48.
(37) Drummond, C.; Alcantar, N.; Israelachvili, J.; Tenne, R.; Golan, Y. Microtribology and Friction-Induced Material Transfer in WS_2 Nanoparticle Additives. *Adv. Funct. Mater.* **2001**, *11*, 348−354.
(38) Praveena, M.; Bain, C. D.; Jayaram, V.; Biswas, S. K. Total Internal Reflection (TIR) Raman Tribometer: A New Tool for *in situ* Study of Friction-Induced Material Transfer. *RSC Adv.* **2013**, *3*, 5401−5411.

DOI: 10.1021/am5083232
ACS Appl. Mater. Interfaces 2015, 7, 3708−3716